buildings

MDPI

Article

Performance and Heavy Metal Analysis of Graphite Tailings Cured Using Cementitious Materials

Ruixin Jiang [1,2] and Zhengjun Wang [1,2,*]

[1] School of Water Conservancy and Electric Power, Heilongjiang University, Harbin 150080, China; 2221981@s.hlju.edu.cn
[2] International Joint Laboratory of Hydrology and Hydraulic Engineering in Cold Regions of Heilongjiang Province, Harbin 150080, China
* Correspondence: 1995073@hlju.edu.cn; Tel.: +86-13604805011

Abstract: The massive accumulation of graphite tailings causes serious environmental pollution, mainly from heavy metal pollution. Therefore, this article introduces a method of using graphite tailings as a high-content main material, cement as a small component of the auxiliary cementitious material, and clay as a substitute for cement. The compressive strength and permeability of graphite tailing–solidified material (GT, GT–Clay) were tested, and the effect of clay partially replacing cement as an auxiliary cementitious agent on GT–Clay performance was compared. In addition, inductively coupled plasma mass spectrometry (ICP) was used to analyze the effect of the graphite tailing placement time on the heavy metal content, as well as the changes in the GT heavy metal leaching concentration and its heavy metal content under outdoor freeze–thaw conditions. Scanning electron microscopy (SEM) and X-ray diffraction (XRD) were used to elucidate the microstructural changes in the GT–Clay. The experimental results show that, as the substitution of clay for cement increased from 0 to 50%, the compressive strength of the 90% GT–Clay gradually decreased, and the permeability also increased. The compressive strength of 95% GT–Clay did not show significant changes, but the permeability increased, and when mixed with quicklime, gypsum, and silica fume, the permeability decreased. The Ni and As in graphite tailings fluctuated significantly with the placement time. The heavy metal leaching concentrations of the 90% GT and 95% GT were below the standard limit, and Cd, As, and Ni in GT were potential sources of pollution. The analysis of the microscopic test results showed that the hydration products of the GT–Clay included ettringite, $Ca(OH)_2$, and calcium silicate hydrates. The hydration product stabilized and filled the gaps between the tailing particles, thereby cementing them together. Not only did it improve the mechanical strength of GT, it also reduced the permeability and heavy metal leaching rate. This study provides a new analytical approach to applying graphite tailings for environmental treatment.

Keywords: graphite tailings; curing treatment; compressive strength; permeability coefficient; heavy metal leaching

Citation: Jiang, R.; Wang, Z. Performance and Heavy Metal Analysis of Graphite Tailings Cured Using Cementitious Materials. *Buildings* **2024**, *14*, 537. https://doi.org/10.3390/buildings14020537

Academic Editors: Peilong Li, Zhan Ding and Xiuming Jiang

Received: 9 January 2024
Revised: 2 February 2024
Accepted: 8 February 2024
Published: 17 February 2024

1. Introduction

Graphite is a nonmetallic material that is indispensable to today's high-tech military and modern industrial development [1,2], and is mainly mined in China, India, and Brazil [3]. Due to its good natural floatability, all graphite can be purified using flotation [4]. However, 1 ton of graphite produces 10–15 tons of graphite tailing sand [5]. At the same time, due to the natural graphite ore in the flotation process being mixed with a large number of complex toxic heavy metals, such as As, Ba, Cd, Cr, Cu, Ni, Pb, Se, and oxygenated anions [6], the massive accumulation of graphite tailings not only wastes land resources, but also causes heavy metal pollution in the soil and water around the mine [7,8]. Under the influence of long-term heavy metal pollution in the soil around the graphite tailing sands, heavy metals have been accumulating in the soil and migrating

to deeper layers, leading to more serious deep soil pollution and adversely affecting plant growth [9]. Therefore, the effective recycling of graphite tailings is significant for environmental protection research. At present, graphite tailings are being applied in the field of building materials, such as environmentally friendly concrete and pavements material [10,11]. Fu et al. [12] prepared a graphite tailing sand–semi-coke composite anode with a high multiplication rate, long cycle life, and low cost, thereby realizing the high-value utilization of graphite tailing sand. Hu et al. [13] used graphite tailings as a raw material to prepare foamed ceramics through the high-temperature self-foaming method, which is also an economic treatment for graphite tailings. However, this is still not enough to satisfy the large utilization of graphite tailings for recycling [14].

Curing technology is an effective method for dealing with heavy metals in tailings, and silicate cement has become a commonly used curing agent for waste curing due to its high strength and the prevalence of the required raw materials [15]. However, reducing the amount of cement has become a key objective due to the high production cost and the production of a high number of pollutants such as CO, which consumes energy and pollutes the environment [16]. Related studies, such as that of Feng et al. [17], using cement stabilization to solidify antimony mine tailings concluded that with a higher tailing content (75% and 90%), the mechanical strength and heavy metal immobilization capacity decreased significantly. Yong et al. [18] stabilized and cured lead and cadmium tailings through a clinkerless binder, reducing the amount of cement used and lowering the cost of the cement used. The partial replacement of cement by using clay minerals as supplementary cementitious materials is now recognized as an effective way to reduce the harmful environmental impact of cement [19]. Clay has good plasticity and combines with water to form agglomerates, which have a certain cohesive force that fills the pores in the structure. However, water loss causes the soil to shrink and causes cracks. Compared with cement, clay has a certain weak bonding effect on graphite tailings [20,21]. Juntao et al. [22] studied the partial replacement of cement with heat-treated waste marine clay and found that a replacement rate of 15% had the best performance, and the mechanical properties of the mortar were weakened by a replacement rate of more than 45%, with the pore space increasing and the agglomeration effect not being obvious. This proves the feasibility of clay as an auxiliary cementitious material. After a considerable amount of research and effort, the authors proposed a GT preparation method that is mainly based on graphite tailing sand and utilizes tailing cement filling technology to properly mix cement, clay, water, and tailing to form a filling slurry, which is then transported to the underground mining area through a pumping system so that the graphite tailing sand can be consumed in high quantities without harming the environment.

At present, there is relatively little research on how to deal with graphite tailings in high quantities according to the economic benefits, and research on how to ensure the environmentally sound treatment of graphite tailings is not extensive enough to further explore how to produce a good curing effect on graphite tailings with a small amount of silicate cement, ensuring that the treatment is harmless. Using the basic physical properties of graphite tailings, we focused on the compressive strength and permeability of graphite tailings under the joint action of cement and clay, and we explored the changes in the heavy metal leaching concentrations of GT under different cement dosages. We also studied the microstructure of GT and GT–Clay under different cement dosages by adopting microscopic test methods, such as XRD, XRF, and SEM, so as to provide a theoretical basis for the engineering application of the harmless and resourceful treatment of graphite tailing sands (the preparation of filler works of graphite tailing sands and road subgrade materials).

2. Experimental Programs

2.1. Raw Materials

Based on the principle of solid waste to maximize the utilization of resources, the raw materials selected for the experiment were graphite tailing, clay, and ordinary Portland cement. The graphite tailings and clay were sourced from Luo Bei County, Hegang City, Heilongjiang Province, China. The clay sample was passed through a 0.5 mm sieve and dried in a 105 °C oven for the corresponding experiments. The basic physical properties of the graphite tailings and clay are shown in Table 1. The chemical composition and XRD patterns of the graphite tailings and clay are shown in Figures 1 and 2. A comparative analysis of the particle size distribution of graphite tailings, clay, and cement is also shown in Figure 3. The main chemical composition of graphite tailings used in the test included SiO_2, SO_3, Al_2O_3, CaO, and Fe_2O_3, of which the content of SiO_2 was as high as 48%. The main chemical composition of clay included SiO_2, Al_2O_3, Fe_2O_3, K_2O, of which the content of SiO_2 was as high as 63.5%. By analyzing the diffraction peaks in the XRD patterns, it was found that the SiO_2 in the graphite tailings mainly existed in the form of quartz minerals. In addition, characteristic peaks of plagioclase feldspar, muscovite, calcite, and hematite were found. The SiO_2 in clay XRD mainly exists in the form of quartz minerals, exhibiting characteristic peaks of clay minerals such as illite and kaolin. The diffraction peak results were basically consistent with the chemical composition obtained from the XRF analysis. The graphite tailing sand and clay, as well as the cement particles, were examined using a Malvern laser particle sizer, and the specific surface areas of the graphite tailing sand, clay, and cement were found to be 23.07 m^2/kg, 67.97 m^2/kg, and 75.70 m^2/kg, respectively, indicating that the clay and cement were finer.

Table 1. Properties of graphite tailings and clay.

Graphite Tailings	Water Content	Bulk Density kg/m^3	Apparent Density kg/m^3	Porosity
	5.18%	1450	2857	49.2%
Clay	**Liquid limit**	**Plastic limit**	**Plasticity Index**	
	41.983%	26.50	15.483%	

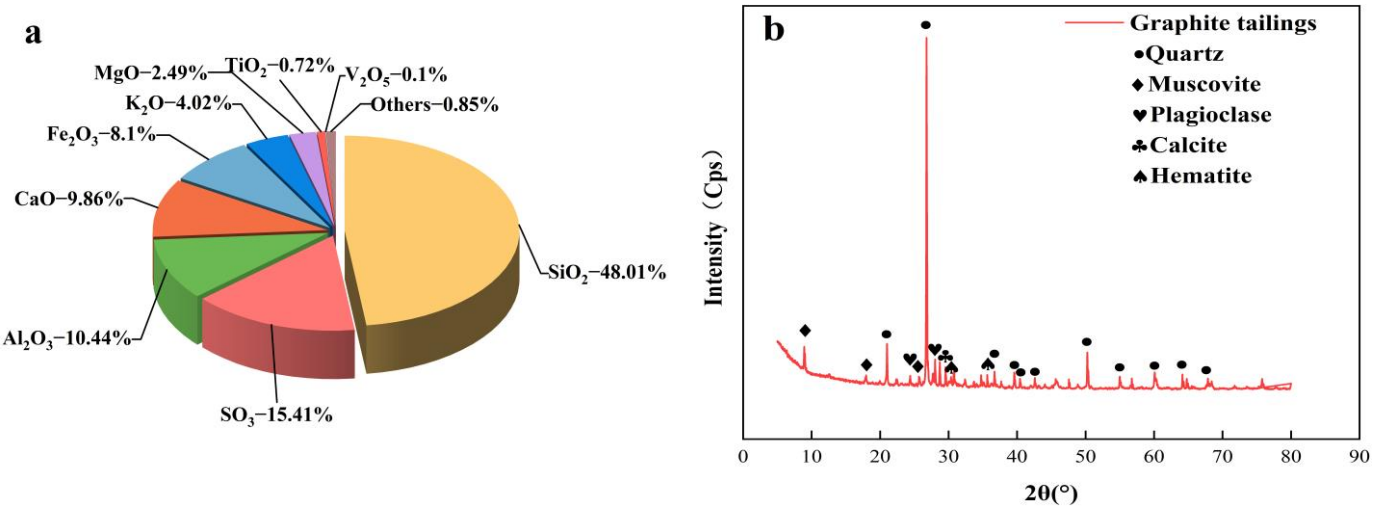

Figure 1. XRF analysis result (**a**) and XRD pattern (**b**) of graphite tailings.

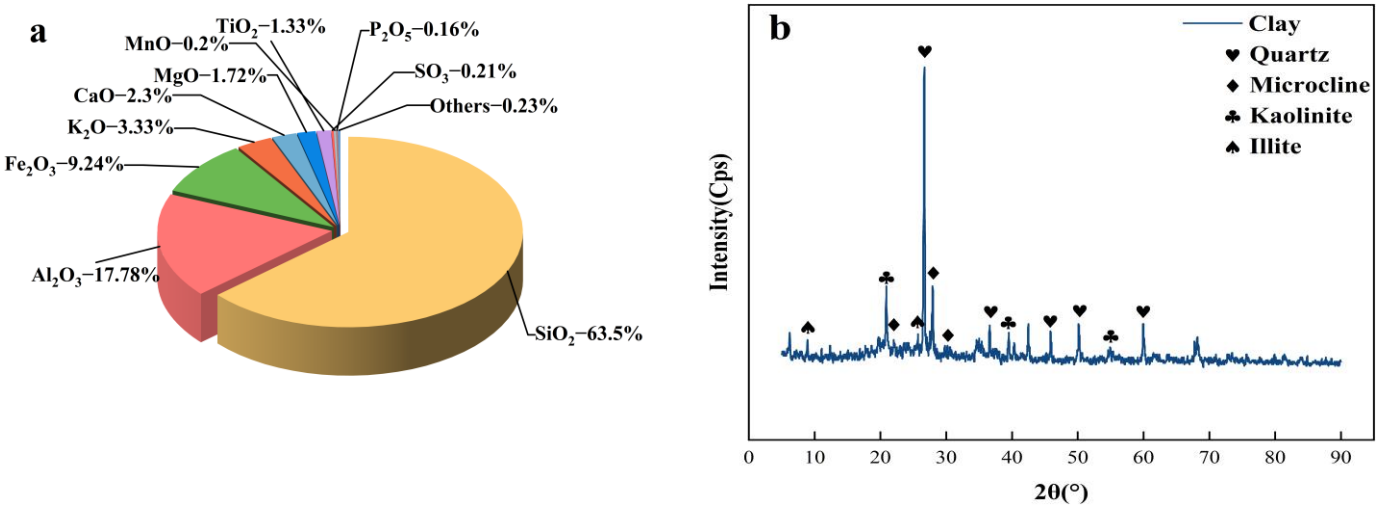

Figure 2. XRF analysis result (**a**) and XRD pattern (**b**) of clay.

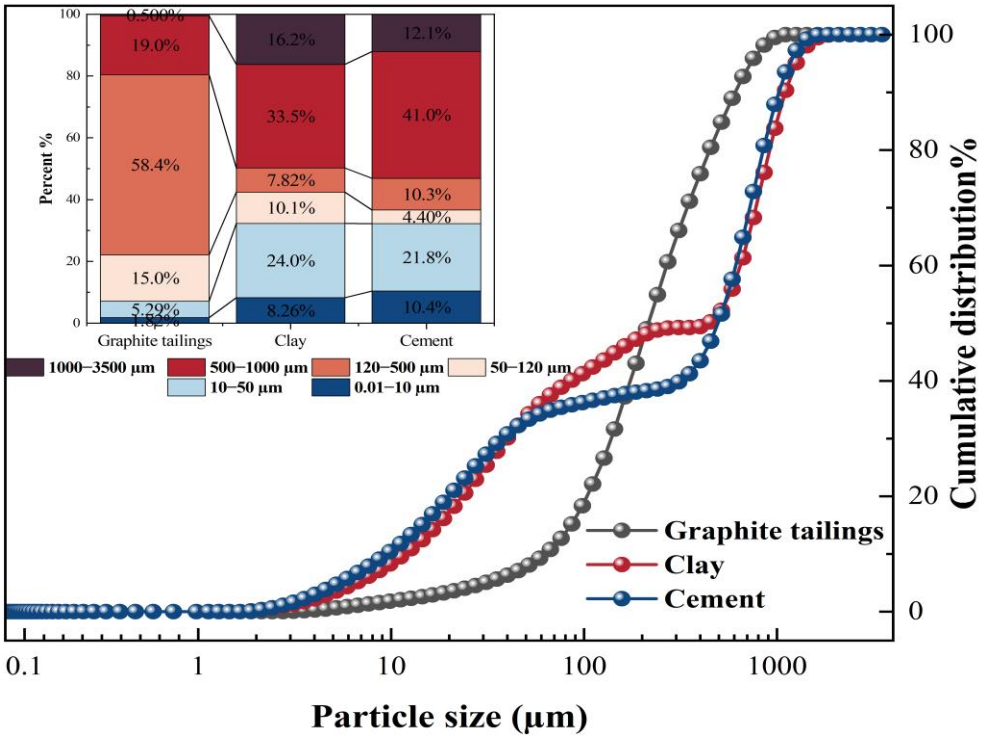

Figure 3. Graphite tailings, clay, and cement particle size distribution.

2.2. GT Preparation

The cement GT specimens were prepared as follows: first, in order to control the moisture content in the tailing sand, the graphite tailing sand was spread to a ventilated and dry place and naturally air-dried for 24 h. Then, the graphite tailing sand was mixed with the cement in a concrete mixer for 60 s, and an equal amount of water was added in two additions, each time mixing for 60 s, for a total of 180 s. When the mixing was completed, the GT was poured out. Then, the cured material was injected into a standard plastic mold with dimensions of 100 × 100 × 100 mm and placed on a vibrating table to be vibrated. Finally, the top of the mold was scraped off with a spatula. To prevent moisture loss in the GT, the surface was covered with plastic wrap. Argane, R. [23] showed that it is possible that the heavy metals in the tailing sand delayed the hydration of the cement by forming a low permeability layer around the incompletely hydrated particles in the

cement, thus prolonging the setting time of the cured mass. Therefore, the early setting and hardening rate was slow, and it was necessary to wait for 48 h before removing the mold in order to minimize the impact of surface spalling and cornering in subsequent experiments. After demolding, the sample was placed into the standard curing room, with a constant temperature of 20 ± 0.5 °C and humidity of 95% ± 5% for the corresponding age. Table 2 shows the specific mixing ratios of the graphite tailings cured with cement as an auxiliary cementitious material (GT).

Table 2. Mixing proportions of GT.

Samples	Graphite Tailings (wt%)	Cement (wt%)	W/S
85% GT	85	15	0.19
90% GT	90	10	0.19
91% GT	91	9	0.19
92% GT	92	8	0.19
93% GT	93	7	0.19
94% GT	94	6	0.19
95% GT	95	5	0.19

Note. GT (wt%) = graphite tailings/(graphite tailings + cement). W/S = water/(graphite tailings + cement).

The clay–cement GT specimens were prepared as follows: after taking the soil samples that passed through a 0.5 mm sieve, they were dried in an oven at 105 °C, and the above steps were repeated. Table 3 shows the specific mix proportions of graphite tailings cured using the clay replacement of cement-assisted cementitious materials (GT–Clay).

Table 3. Mixing proportions of GT–Clay.

Samples	Graphite Tailings (wt%)	Clay (wt%)	Cement (wt%)	W/S
90% GT–0% Clay	90	0	10	0.19
90% GT–10% Clay	90	1	9	0.19
90% GT–20% Clay	90	2	8	0.19
90% GT–30% Clay	90	3	7	0.19
90% GT–40% Clay	90	4	6	0.19
90% GT–50% Clay	90	5	5	0.19
95% GT–0% Clay	95	0	5	0.19
95% GT–10% Clay	95	0.5	4.5	0.19
95% GT–20% Clay	95	1	4	0.19
95% GT–30% Clay	95	1.5	3.5	0.19
95% GT–40% Clay	95	2	2	0.19
95% GT–50% Clay	95	2.5	2.5	0.19

Note. GT–Clay (wt%) = graphite tailings/(graphite tailings + cement + clay). W/S = water/(graphite tailings + cement + clay).

2.3. Experimental Methods

The experimental plan is shown in Figure 4, and the test details are described in the following subsection.

2.3.1. Macro-Property Testing Methods

Compressive Performance Test

The determination of GT's compressive strength was performed according to the Chinese standard JGJ/T70–2009 [24]. Respectively, the dosages were 85%, 90%, and 95% graphite tailing sand for 7 d, 14 d, 28 d, and 60 d, with constant temperature and humidity standardization. The pressure test machine was used for pressure testing, with the average value taken from three tests. Based on the economic benefits, clay replaced cement with 90% and 95% graphite tailings, with substitution rates of 0%, 10%, 20%, 30%, 40%, and 50%, respectively. The changes in the compressive strength of the GT–Clay were analyzed.

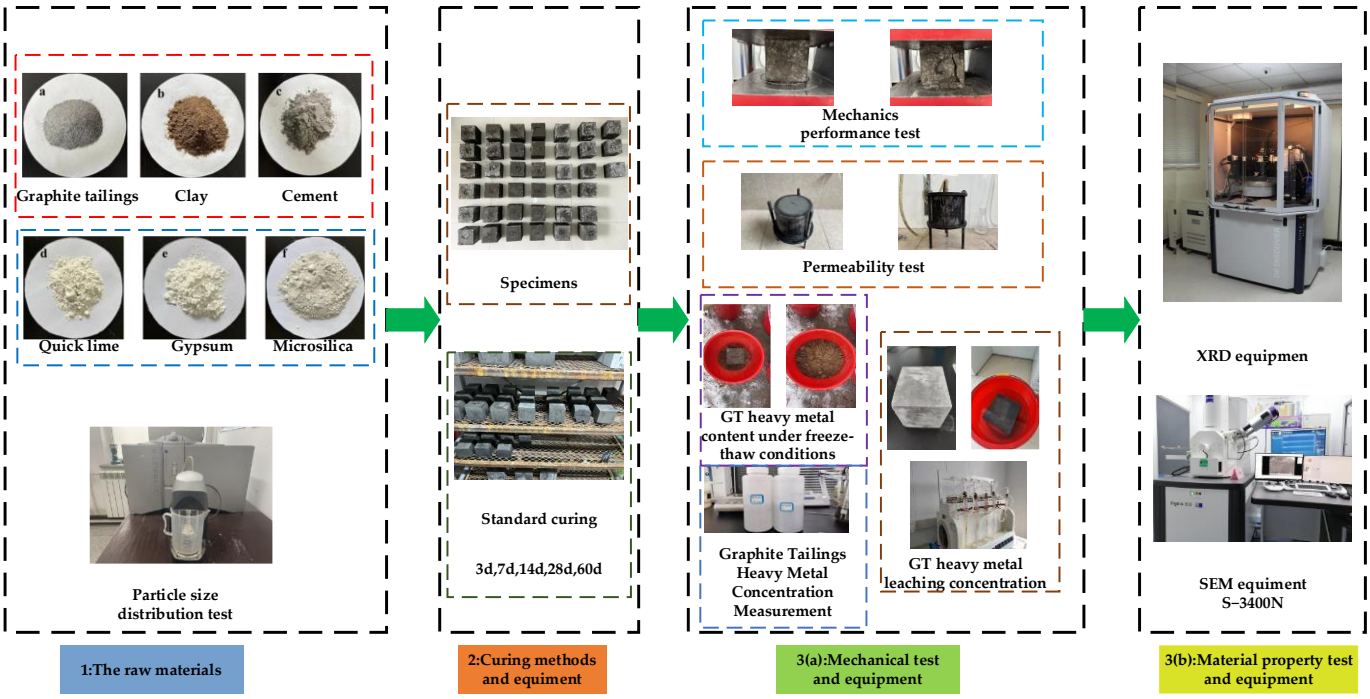

Figure 4. Flowchart of experimental methods.

Penetration Performance Testing

The determination of the GT permeability coefficient was performed according to the Chinese standard GB/T50123–2019 [25]. For the Variable Head Infiltration Test Method, the GT specimen was made of a cylinder with a diameter of 10 cm and a height of 10 cm. During the test, the test head gradually decreased, and according to D'Arcy's law, the flow rate passing through the curing material during the test time t was equal to the amount of water decreasing in the variable head pipe. The variable head pipe's head-down speed and time relationship was determined according to the following formula and was used to calculate the permeability coefficient of the curing material k_T. The permeability coefficient sas based on Equation (1).

$$k_T = 2.3\frac{\mathrm{aL}}{\mathrm{A}t}\lg\frac{H_{b1}}{H_{b2}} \quad (1)$$

where k_T is the permeability coefficient of the specimen at water temperature T °C (cm/s); a is the cross-sectional area of the variable head pipe (cm^2); L is the seepage diameter (cm); and H_{b1} and H_{b2} are the beginning head and the termination head (cm), respectively.

2.3.2. Material Characterization Tests

Heavy Metal Leaching Test

According to GB5085.3–2007 [26], a leaching experiment on heavy metals from GT was carried out, and the pre-treatment utilized HJ/T299–2007 [27]. The leaching agent was added according to a liquid–solid ratio of 10:1, and then the bottle was fixed on the flip-type oscillator after tightening the cap. The rotational speed was adjusted to (30 ± 2) r/min, and the oscillation was carried out at (23 ± 2) °C for (18 ± 2) h. The leaching solution was filtered using a pressure filter, the filtrate was collected, and the concentration of heavy metals in the leaching solution was determined. The leachate was filtered through a pressure filter, and all of the filtrate was collected to determine the concentration of heavy metals in the leachate. The heavy metal concentrations in the graphite tailings and GT leachate were determined via inductively coupled plasma mass spectrometry (ICP–MS, 7900/16–32).

Material Characterization Tests

Scanning electron microscopy (SEM) involves the use of an electron gun that emits an electron beam after focusing on the surface of the specimen for raster-like scanning. The detection is performed by electrons interacting with the specimen generated by the signal on the surface, including its composition, morphology, and structure [28]. The 28 d compressive strength determination specimen was crushed. The selected curing material was a small specimen. The specimen was intended to be as flat as possible, in small pieces. The specimen was placed into a sealed bottle with an anhydrous ethanol soak to stop the specimen from continuing to hydrate. During the microscopic test, the specimen was taken out of the bottle, dried at 45 °C to a constant weight, and then placed in the SEM specimen carrier plate for gold spraying. Then, it was placed under the scanning electron microscope for observation.

3. Results and Discussion

3.1. Compressive Strength Analysis

3.1.1. Influence Law of GT Compressive Strength

Water, graphite tailing sand, and cement were adapted according to the above proportions and set as the initial mix ratio. Figure 5a reflects the curve of the effect of age on the GT compressive strength of graphite tailing sand with different dosages. There were significant differences in compressive strength for 85% and 90% GT at different ages. For 95% GT, it was not obvious; as the proportion of graphite tailing sand continued to increase, the proportion of cement per unit volume decreased accordingly and was unable to generate relatively dense hydration products, resulting in the 95% GT compressive strength change being insignificant. When the cement content was greater than 10% (15% in this test), the compressive strength increased sharply. After 60 d of maintenance, the strength value reached 6.67 Mpa, which is the same maintenance conditions under the same cement content of 5% (0.37 Mpa) maintained for 7 d 17.81 times. Hence, the maintenance age of the high-cement-content doping specimen strength growth was more significant. The prolongation of the curing age made the hydration reaction of many cementitious materials within the GT specimens more complete, generating more calcium silicate hydrate and significantly improving its compressive strength [29]. The graphite tailing sand compressive strength data results of different dosages were fitted using linear regression equations through the Origin software, and the graphite tailing sand dosage–compressive strength relationship is shown in Figure 5b. For the same maintenance age of 28 days, for different graphite tailing sand dosages, the compressive strength of GT with a high cement dosage was stronger, consistent with the above conclusion. According to Quan's [30] research, the optimal replacement rate of graphite tailings was 50%, which was far from enough to handle a large amount of graphite tailings. Therefore, a compressive strength analysis was conducted on GT with a content of 85–95%. It was found that the content of graphite tailings significantly impacted the compressive strength. The higher the content of graphite tailings, the lower the compressive strength. This was because the accumulation effect of graphite tailing particles could not compensate for the decrease in the effective hydration amount of the cementitious material when the cementitious material was low, resulting in a decrease in compressive strength. According to the trend of compressive strength variation, GT with content between 85% and 90% can be selected, with a compressive strength between 2.5 Mpa and 5.5 Mpa, which meets the economic requirements of using a small amount of cement and basic mechanical properties.

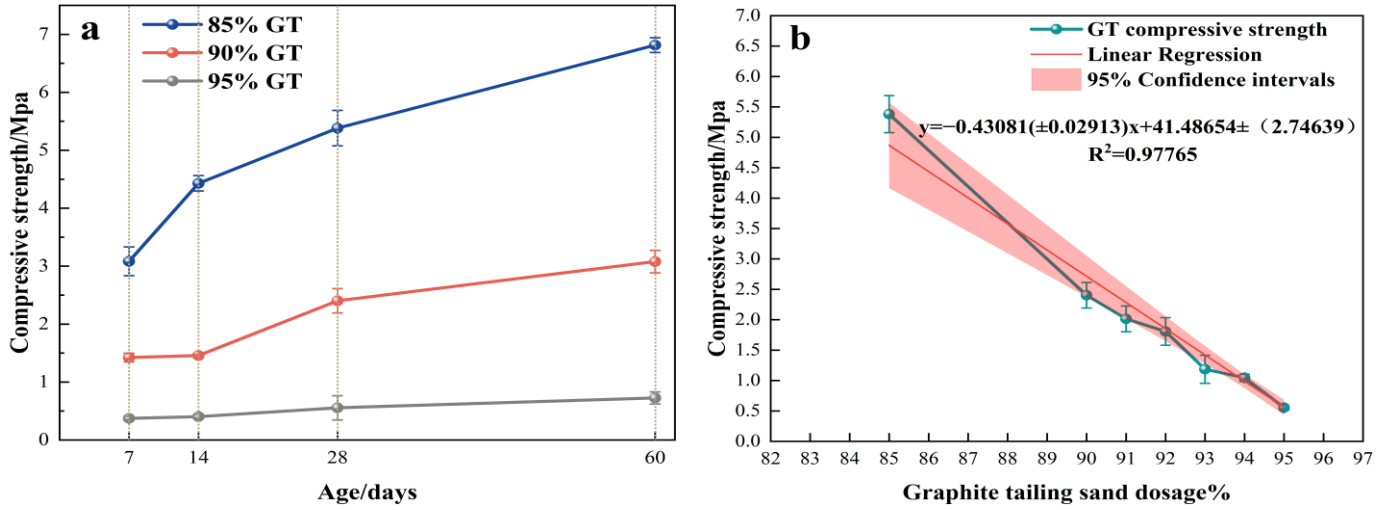

Figure 5. (**a**) Effects of different ages on GT compressive strength; (**b**) effects of different graphite tailing sand admixtures on GT compressive strength.

3.1.2. Influence Law of GT–Clay Compressive Strength

Keeping the 90% and 95% GT ratios unchanged, to study the effect of different substitution amounts of clay on the compressive strength of GT, the clay replaced 0%, 10%, 20%, 30%, 40%, and 50% of the cement mass; the results are shown in Figure 6a,b. The strength activity index is the ratio between the average compressive strength of the GT samples with clay partially replacing cement and the average compressive strength of the control group [31]. The 90% graphite tailing sand substitution rate gradually decreased the compressive strength with the increase in clay and the decrease in cement. The 40% clay substitution rate was the lowest, and its compressive strength decreased by 63.2% compared to the 0% clay substitution rate of graphite tailing sand. The strength of 90% GT–Clay is mainly provided by the hydration products generated by the reaction between cement and water. With the gradual decrease in cement dosing, the amorphous C–S–H gel could not continue to cement the graphite tailing sand particles. This led to a decrease in the compressive strength of 90% GT–Clay, with an increased clay substitution rate.

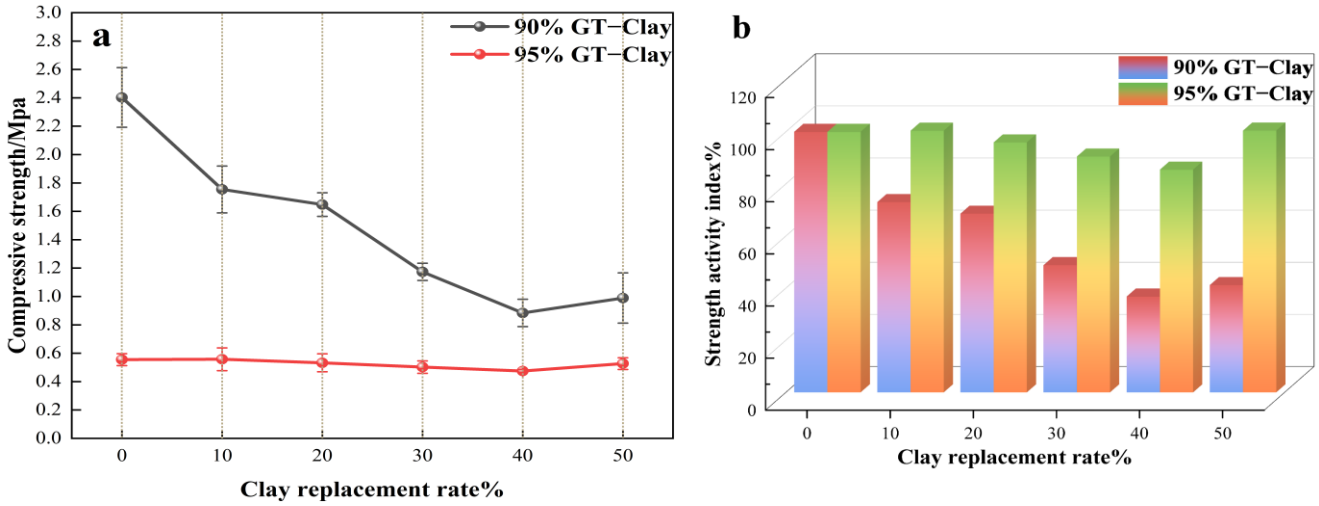

Figure 6. (**a**) Effect of GT–Clay compressive strength with different clay substitution rates; (**b**) effect of GT–Clay strength activity index with different clay substitution rates.

In 95% GT–Clay, the low cement dosing and low clay dosing resulted in the content of clay and cement in GT–Clay not changing much as the clay substitution rate increased, and the internal hydration products did not change much, either. Therefore, the compressive strength of 95% GT–Clay was at a stable minimum of 0.5 MPa with increasing clay substitution. The correlation coefficient R^2 of the fitted curve of clay–cement GT compressive strength with the clay substitution rate was not less than 0.95, which indicates that the fitted curve was very similar to the change rule of clay–cement GT compressive strength in the text.

3.2. Analysis of Permeability Coefficients

GT–Clay Impermeability Properties

Figure 7 provides the relationship between the clay replacement rate and GT permeability coefficient; with the increase in the clay substitution rate, the pore space of the GT–Clay skeleton increased gradually, and the permeability was enhanced. The 90% GT–Clay curve can be divided into three stages: clay substitution rate <10%, substitution rate = 10–20%, and substitution rate >20%. When the clay substitution rate was between 0% and 10%, the hydration reaction dominated, and a small amount of water combined with the clay, leaving the clay in a plastic state with increased cohesion. Clay agglomerates filled the pores in the cured body while compensating for the negative effects of reduced cement hydration products, and the permeability of the GT–Clay tended to stabilize. When the clay substitution rate was between 10% and 20%, water and cement hydration occurred, and the combination of clay and water was in the liquid state. The water film formed a lubricant on the clay surface, reducing the friction between the particles and electrostatic molecular attraction; the cohesion decreased sharply, and the number of agglomerates decreased. When the hydration product decreased, the pore space of the curing body increased, and the permeability of GT–Clay increased sharply. When the clay substitution rate was between 20% and 50%, a large amount of clay combined with water, and the clay was back in the plastic state, enhancing the friction and electrostatic molecular attraction between the particles. The combination with water formed agglomerates that filled the pores within the curing body, but as the reduction in cement led to a reduction in amorphous C–S–H gels, the clay was unable to eliminate the negative effects of the reduction in hydration products, and the permeability of GT–Clay slowly increased [21]. According to the "general industrial solid waste storage and landfill pollution control standards" (GB18599–2020) [32] in the first category of general industrial waste landfill standards, the natural saturation permeability coefficient of the solidified material should not be greater than 10^{-5} cm/s. The 90% GT–Clay with the clay substitution rate and the permeability coefficient increased gradually, but the permeability of the landfill to meet all the above requirements could be determined.

In the 95% GT–Clay curve, although the clay substitution rate gradually increased, the clay did not effectively form agglomerates with water due to the increase in the graphite tailing sand content compared to the 90% GT–Clay. The cement content gradually decreased, and the hydration product gradually decreased, resulting in a gradual increase in pore size, a gradual increase in permeability coefficient, and a coefficient of permeability greater than 10^{-5} cm/s. The 95% GT–50% clay, compared to the natural saturated permeability coefficient of 10^{-5}, increased by 319%, which is consistent with the conclusion of Yuxian Ke [33]. More graphite tailings and fewer cementitious materials made the cured mass micropores looser and more porous, resulting in more microcracks and pores that connected to form defects, enhancing the penetration properties of its cured mass.

Figure 8 compares the permeability properties of 95% graphite tailing sand, 2.5% cement, and 2.5% clay with 5% quicklime, gypsum, and silica fume, respectively. In this experiment, quicklime, gypsum, and silica powder comprised 5% of the total cementitious material. Meanwhile, comparing the water absorption rate of the different graphite tailing sand specimens, the external lime curing material had the lowest amount of water absorption, indicating that, at this time, the diffusion of water in this curing material was the

lowest, the cementite structure and surface structure in the curing material was the most dense, and the lime curing material had the best impermeability, which is consistent with the permeability coefficient in the above figure. This is mainly because GT–Clay is a porous material, the porosity is relatively large, and the addition promoted the hydration reaction of the cementitious material, which made the GT–Clay dense and decreased the porosity. The number of connected pores consequently decreased, leading to the reduced water absorption of the cured material, and the permeability was reduced. Thus, the addition of quicklime, gypsum, and silica fume decreased the permeability of GT–Clay, among which quicklime had the most obvious effect.

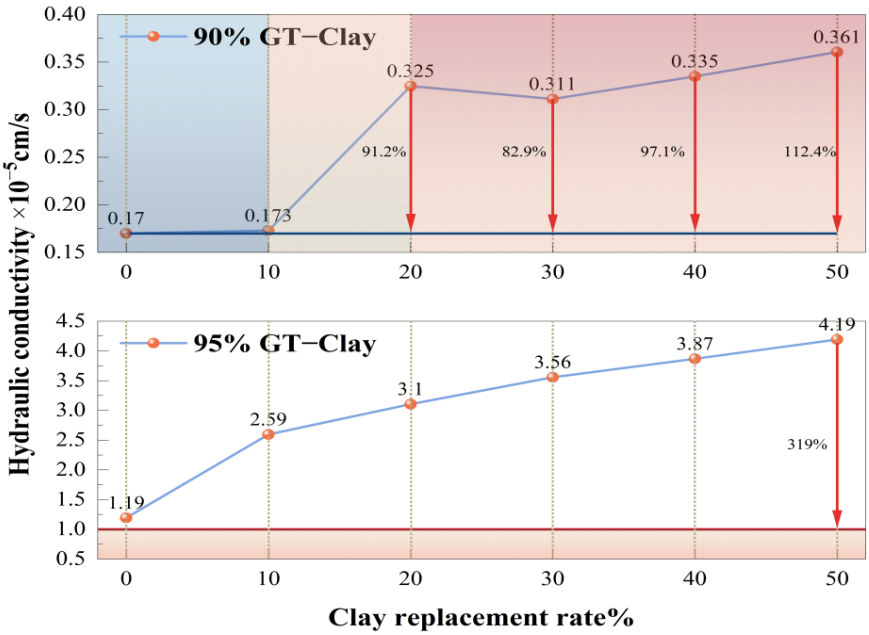

Figure 7. GT–Clay permeability coefficient.

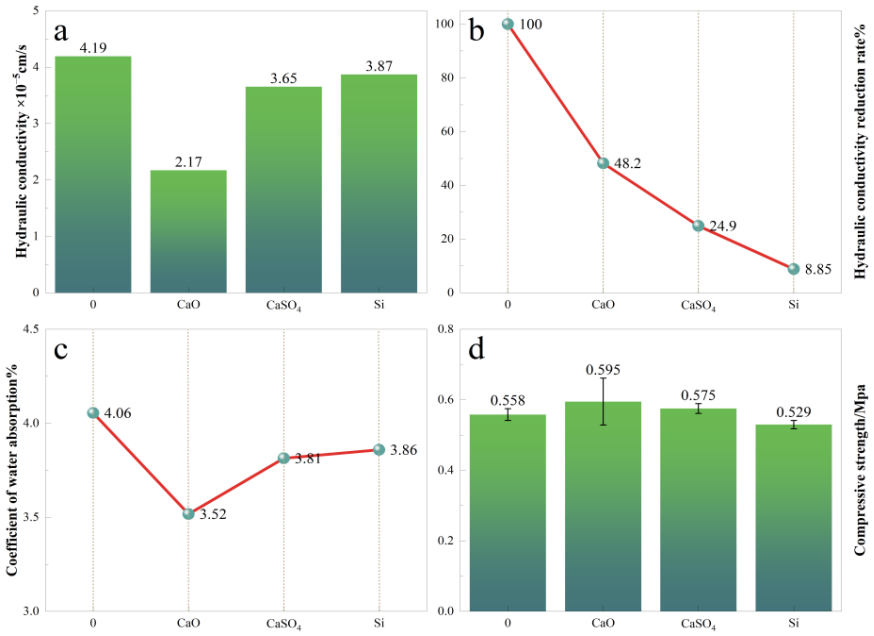

Figure 8. Effects of different external dopants on GT–Clay performance. (**a**) Hydraulic conductivity, (**b**) hydraulic conductivity reduction rate, (**c**) coefficient of water absorption, and (**d**) compressive strength.

The main component of quicklime is CaO. First, a CaO and graphite tailing sand mixture of the water hydration reaction occurs, generating slaked lime $Ca(OH)_2$, and cement in the SiO_2 and Al_2O_3 volcanic ash reaction occurs. This generates C–A–H (calcium aluminate hydrate) and C–S–H (calcium silicate hydrates), filling the pores in the curing of the material between the curing of the graphite tailing sand to become more dense and improve the permeability of the curing of the material. Its chemical reaction equation can be expressed as follows [34,35]:

$$SiO_2 + Ca(OH)_2 + nH_2O = CaO{\cdot}SiO_2{\cdot}(n+1)H_2O \quad (2)$$

$$Al_2O_3 + Ca(OH)_2 + nH_2O = CaO{\cdot}Al_2O_3{\cdot}(n+1)H_2O \quad (3)$$

The soluble component of gypsum, $CaSO_4$, quickly dissolved in water, and under the hydrothermal reaction conditions in the solution of Ca^{2+}, OH^- and $SO_4{}^{2-}$ diffused to the surface of the cement—the clay—so that the activity of SiO_2 and Al_2O_3 was dissolved. Then, C–S–H gel and ettringite (AFt) AFt colorless columnar crystals were generated in the early stage of the reaction of the hydration of heat in the C–S–H gel, and the pore space was filled, thus playing the role of the backbone in the formation of a dense network-like structure [36]. This was because graphite tailings contain high levels of sulfides that impede cement hydration reactions. Gypsum has a positive influence on the volcanic ash effect: an appropriate amount of gypsum can give full play to the volcanic ash effect and improve the negative impact of its sulfides on cement hydration [37,38].

Silica powder is uniformly distributed in GT, and because of its small size, it can fill its internal pores and capillaries to improve the effect of the pore structure, reduce the intrusion of harmful substances, and improve the seepage resistance of the cured material [39].

In summary, all three external admixtures can improve the seepage resistance of their cured materials, and the effect of quicklime is more obvious.

3.3. Heavy Metal Analysis

3.3.1. Graphite Tailing Heavy Metal Analysis

Figure 9a,b show the heavy metal content of graphite tailings for 1–60 days of static placement and quantify the average content concentrations of heavy metal elements in the graphite tailings based on the experimental results of samples obtained from the graphite mining area of Luo Bei, Hegang. Among all of the analyzed elements, Ba had the highest average content concentration of 25.1 ug·L^{-1}; As had a medium average content concentration of 10 ug·L^{-1}; and Cr, Cd, Cu, Ni, Pb, and Se had relatively low average content concentrations, which were under 10 ug·L^{-1}. The maximum and minimum multiples were found for As (4.38 times), and the smallest were found for Pb, Cd (1 time). From the multiplicative relationship, it can be seen that the temporal distribution among the various heavy metals was not uniform. The three heavy metals, Pb, Cd, and Cu, fluctuated less with time, while the other five metal elements fluctuated more, with maximum and minimum multiples of more than one.

According to the classification standard [40], the level of coefficient of variation (CV) can be divided into low variation (CV < 15%), medium variation (15% < CV < 36%), and high variation (CV > 36%). Compared with the standard deviation, the CV can reflect the temporal dispersion and degree of variation of heavy metal elements, and the higher the value, the greater the effect of the time factor on the content of heavy metals. Table 4 shows the changes in the heavy metal precipitation content of graphite tailings during the placement time. The coefficients of variation of Ba, As, and Ni in the graphite tailings were as high as 37.45%, 43%, and 60.91%, respectively, reflecting a high degree of variability, and were significantly affected by the placement time. The coefficients of variation of Cr, Cu, and Se were between 15% and 36%, reflecting medium and weak variability, and were less affected by the time interference. Except for Cd and Pb, the coefficients of variation of the other heavy metal elements were more than 10%, and the data obtained for Ni and As indicated that these elements are more volatile, suggesting that the heavy metal content

in graphite tailings at different times has obvious differences. In general, the average concentration of heavy metal elements in graphite tailing sand in the Hegang Luo Bei graphite mining area is low, and the local graphite tailing sand is highly utilizable.

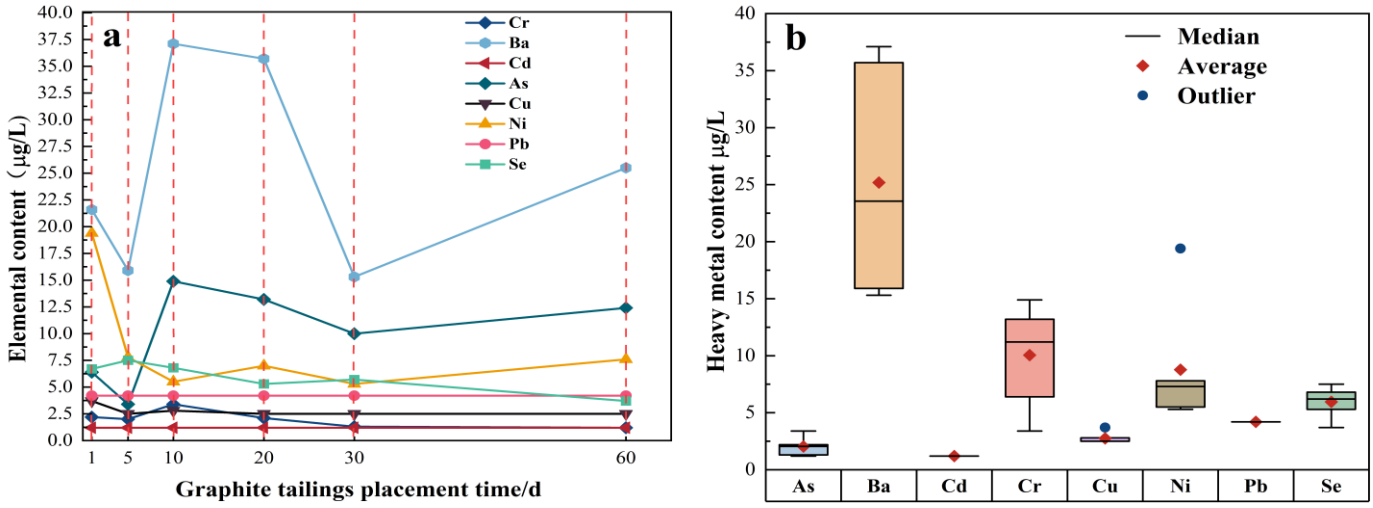

Figure 9. (**a**) Effect of heavy metal changes in graphite tailings with different placement times; (**b**) box plot of heavy metal changes in graphite tailings.

Table 4. Changes in heavy metal precipitation content for graphite tailing placement time.

Parameters	Cr	Ba	Cd	As	Cu	Ni	Pb	Se
Minimum concentration/(ug/L)	1.2	15.3	1.2	3.4	2	5.3	4.2	3.7
Maximum concentration/(ug/L)	3.4	37.1	1.2	14.9	3.7	19.4	4.2	7.5
Average concentration/(ug/L)	2	25.1	1.2	10	2.7	8.7	4.2	5.9
Range/(ug/L)	2.2	21.8	0	11.5	1.2	14.1	4.2	3.8
Standard deviation/(ug/L)	4.39	9.48	0	0.79	0.48	5.31	0	1.36
Highest multiple/(ug/L)	2.84	2.43	1	4.38	1.48	3.66	1	2.03
Coefficient of variation %	35	37.45	0	43	14.81	60.91	0	22.03

Figure 10 shows the correlation analysis of heavy metals in graphite tailings using SPSS data analysis software. The nickel and copper elements showed a strong, significant, positive correlation at the 0.05 level, with a relative coefficient of 0.92. This indicates that the aforementioned heavy metal elements often exist in the form of companion elements or symbiosis, and the sources had a high degree of homology.

3.3.2. GT Heavy Metal Leaching Analysis

Hegang City, Luo Bei County, is located in the northeast of China and has a cold climate, so it is necessary to consider the content and leaching of heavy metals from the GT under freezing and thawing conditions. The above figure simulates the heavy metal content from the GT landfill with soil taken from the local area of Hegang City, Luo Bei County. The GT was covered with soil, an appropriate amount of water was injected into it, and an outdoor freeze–thaw test was conducted for 2 months to analyze the heavy metal content and leaching concentration in the GT. According to the economic benefits, the GT specimens cured with 90% and 95% doping at 28 d of maintenance were selected, as shown in Figure 11a. Whether the graphite tailing sand was combined with cement or not, the leaching concentration of heavy metals was lower than the standard limit, in line with the requirements of the standard (GB5085.3–2007) [26]. Generally speaking, mechanical properties and leaching concentration are the indicators typically used to measure the curing efficiency of heavy metals in cured materials [41]. The compressive strength is inversely proportional to the leaching concentration. There is a significant correlation

between the leaching concentration of heavy metals and the compressive strength of the gelling material, and the higher the compressive strength of GT, the lower the leaching concentration of heavy metals. Among them, the influence of Cr and Ni elements is larger. Further study showed that Cd, Hg, and Ni are the main heavy metal elements that cause soil pollution around graphite tailing ponds, and it can be seen that the curing effect was better and that there was little effect on Ba elements. Therefore, it can be concluded that the cement has a good curing effect on heavy metals in graphite tailing sand, which greatly reduces the leaching of heavy metals. From Figure 11b, it can be seen that the heavy metal content of Cd, As, and Ni in GT was high, much higher than the corresponding soil pollution risk screening value of agricultural land in the national "Soil Environmental Quality Risk Control Standards for Agricultural Land Soil Pollution (Trial)" (GB 15618–2018) [42], indicating that the heavy metal elements in the cured material are released to the surrounding soil and water environment through weathering and leaching; this may cause the soil's heavy metal content to exceed the standard, making it a potential source of heavy metal pollution around the mining area. Thus, for GT curing materials, we should focus on the Cd, As, and Ni elements and their leaching release patterns. Figure 12 demonstrates the micromechanical morphology of heavy metals in cement-cured graphite tailings, where cement hydration encapsulates the heavy metals and the leaching concentration decreases, in agreement with the conclusions drawn in previous work [43].

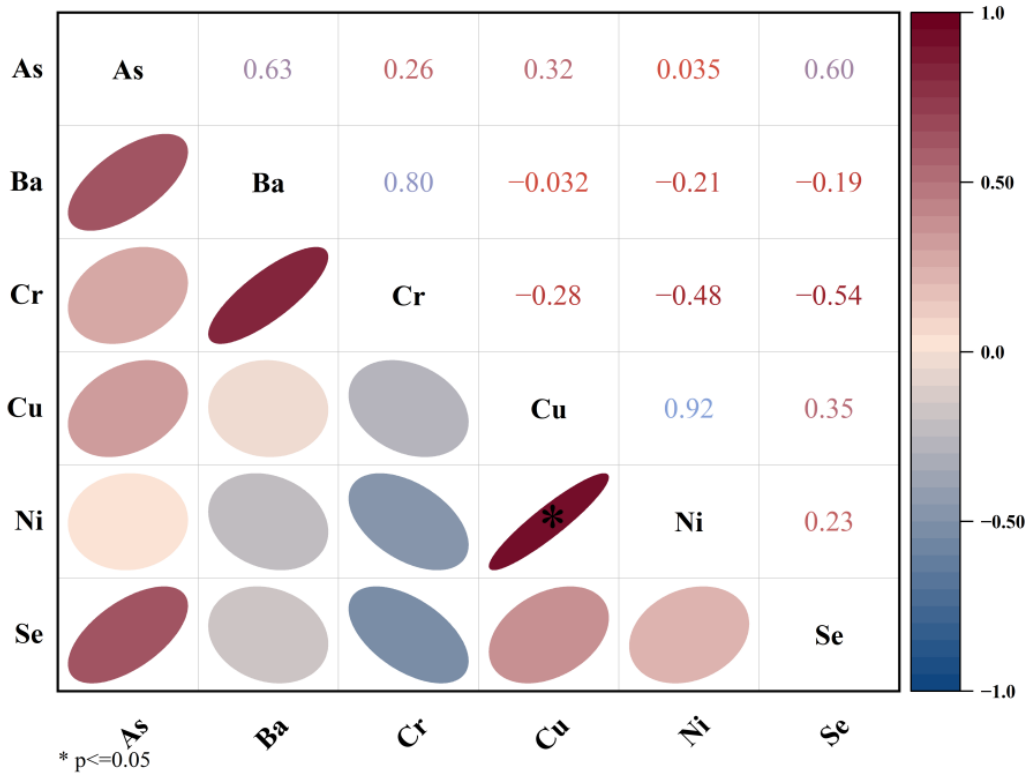

Figure 10. Graphite tailing heavy metal correlation analysis.

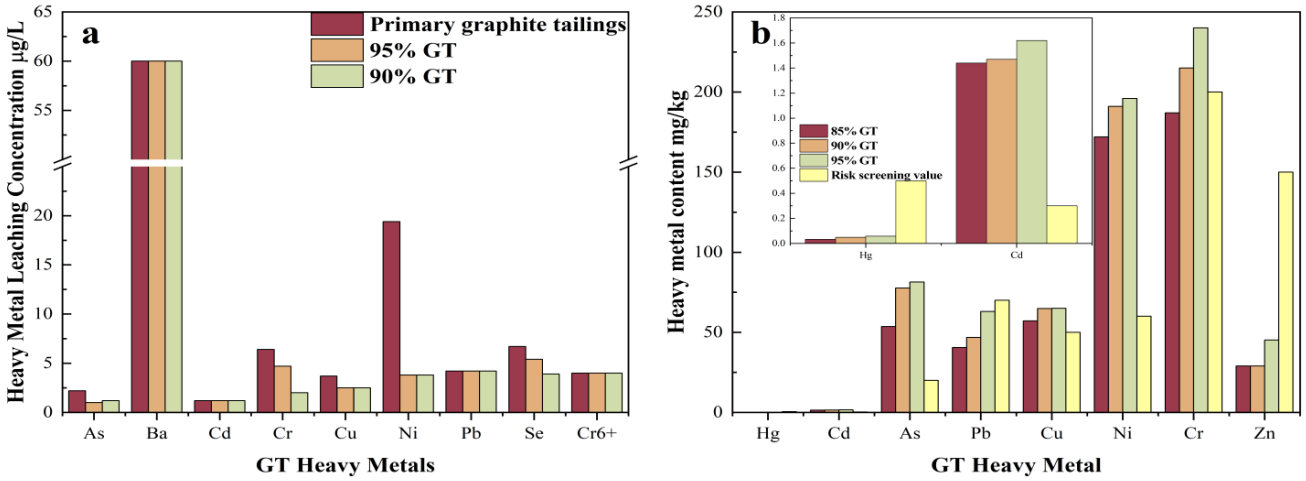

Figure 11. (**a**) GT heavy metal leaching concentrations at different doping levels; (**b**) GT heavy metal content at different doping levels.

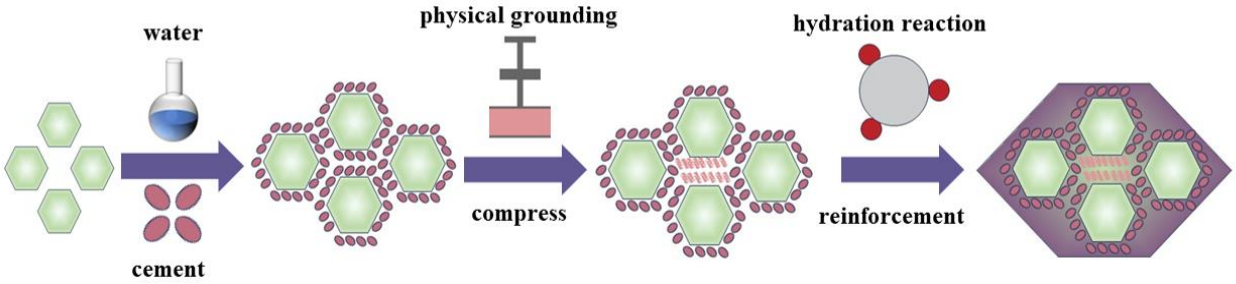

Figure 12. Schematic diagram of graphite tailing curing material.

3.4. Microstructure Analysis of GT–Clay

3.4.1. XRD Analysis

To explore the microscopic mechanism of GT–Clay, Figure 13 shows the XRD diffractograms of 90% GT–50% clay and 95% GT–50% clay maintained for 28 days. The 35°–45° broad peaks correspond to amorphous C–A–S–H gels, which are the main hydration products of silicate cement. This is consistent with the results of other studies [44]. There was no significant change in the minerals of the two samples, and all minerals were dominated by quartz and muscovite diffraction peaks. Due to the high content of graphite tailings in the 95% GT–50% Clay and the limited content of the cement, the curing effect of the graphite tailings was not achieved, resulting in the appearance of broad peaks similar to those of iron and aluminum minerals at around 49° and 80°. The significant change between 90% GT–50% Clay and 95% GT–Clay was the amount of amorphous C–S–H gel produced. Compared with 95% GT–Clay, 90% GT–50% Clay produces more C–S–H gel due to the higher amount of silicate cement, which effectively fills the internal space and improves the pore structure, thus improving its mechanical properties and impermeability. The increased permeability also leads to a decrease in the leaching concentration of heavy metals in the cured body. This is the main reason why 90% GT–50% clay has better impermeability than 95% GT–50% clay [44].

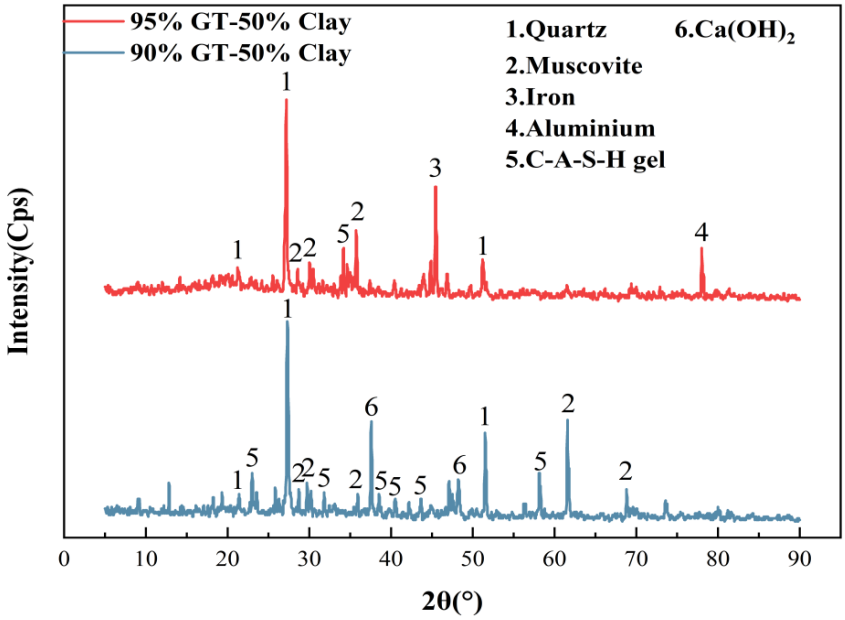

Figure 13. XRD diffractograms of 90% GT–50% clay and 95% GT–50% clay after 28 days of GT–Clay hydration.

3.4.2. SEM Analysis

Since the permeability coefficient of 90% GT–Clay met the requirements, the microanalysis of 90% GT–Clay under different clay substitution rates was also carried out by combining the XRD diffractograms of 90% GT–50% Clay and 95% GT–50% Clay in Figure 13. Figure 14 shows that, with the gradual increase in the clay substitution rate, the cementitious material within the 90% GT–Clay was gradually squeezed until fragmentation; cracks and pore structures gradually developed, and the number of granular objects in the specimens increased, which led to a decrease in the mechanical properties and permeability resistance [45]. From Figure 14a,b, it can be seen that at the clay substitution rate of 0–10%, flaky and flocculent hydration products were found. A small amount of clay was incorporated, water absorption and expansion occurred on the surface of the hydration products, and graphite tailing sand was wrapped around the middle, which improved the densification of the GT–Clay, reduced the porosity within the structure, and compensated for the negative effect of cement reduction. Both the interface and the permeability coefficient were relatively smooth. From Figure 14b,c, it can be seen that when the clay substitution rate was 10–20%, the balance between the cement and clay content gradually broke down. The filling effect of the clay agglomerates in the 90% GT–Clay became saturated, and excess clay existed in the free form in the middle of the cement stone or interface, which hindered the development of the crystalline form of the C–S–H gel and prevented the gel from being bonded to form a three-dimensional structure. The specimen gradually formed holes and caused the permeability coefficient to increase sharply. Figure 14c–f show that the clay content gradually increased, and clay agglomerates gradually replaced the hydration products. Free clay re-formed agglomerates, but due to the presence of fewer hydration products, the increased pore space was not enough to support the original skeleton structure formed by the hydration products, ultimately resulting in a slow increase in the permeability coefficient.

Figure 15 shows more clearly the microstructure of the graphite tailings under the joint action of clay and cement. The active SiO_2 and Al_2O_3 in clay reacted with the $Ca(OH)_2$ in cement during the volcanic ash reaction, which produced agglomeration and generated secondary hydrated calcium silicate and hydrated calcium aluminate with less alkalinity. These generators play an important role in the strength of the specimen [46]. The flocculent

C–S–H gel and rod-shaped calcium alumina in the late hydration GT–Clay, which were interwoven, were filled and tightly bound to each other to make the structure denser.

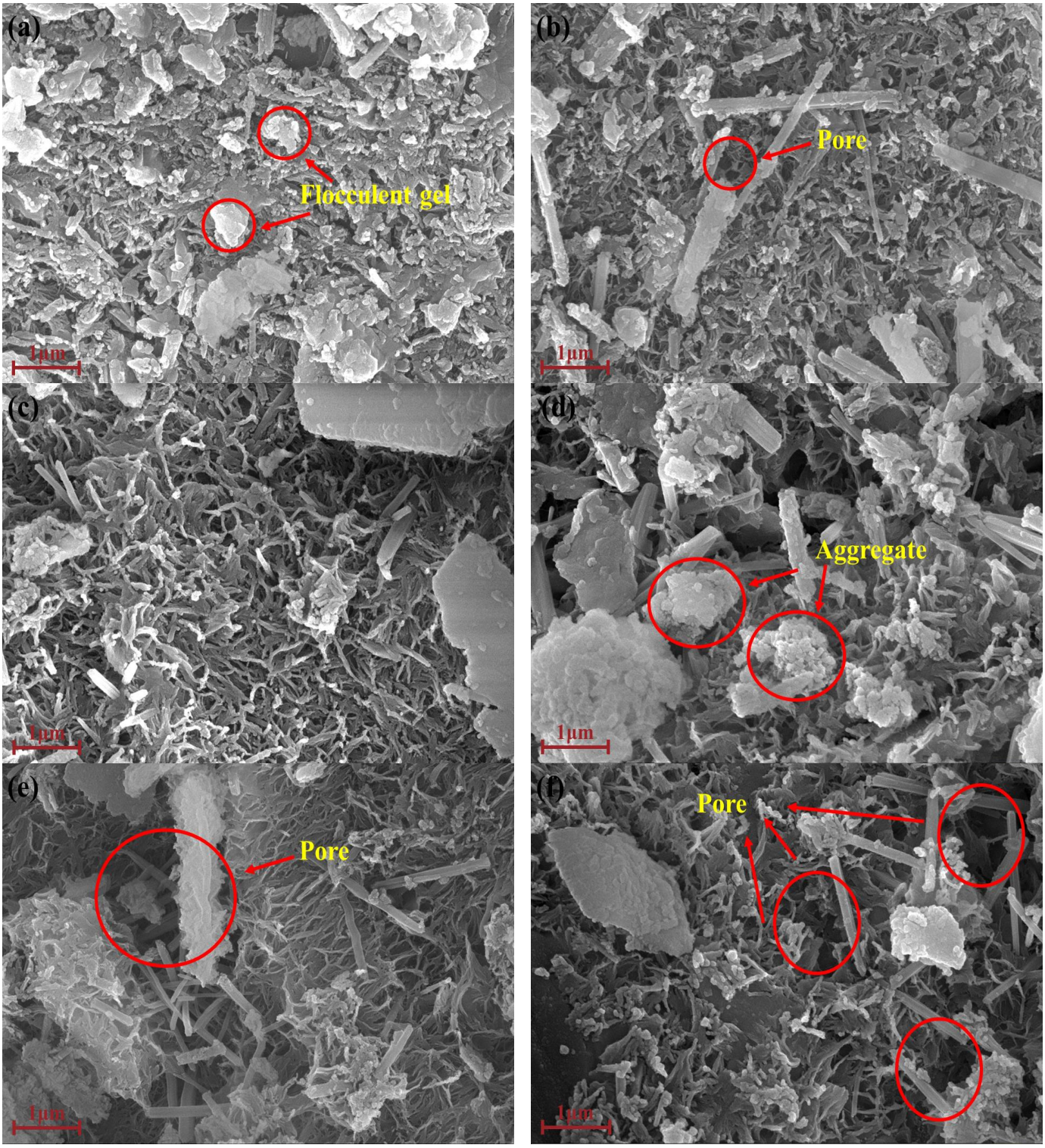

Figure 14. Scanning electron microscope images of 90% GT–Clay at different clay substitution rates. (**a**) 90% GT–0% clay; (**b**) 90% GT–10% clay; (**c**) 90% GT–20% clay; (**d**) 90% GT–30% clay; (**e**) 90% GT–40% clay; (**f**) 90% GT–50% clay.

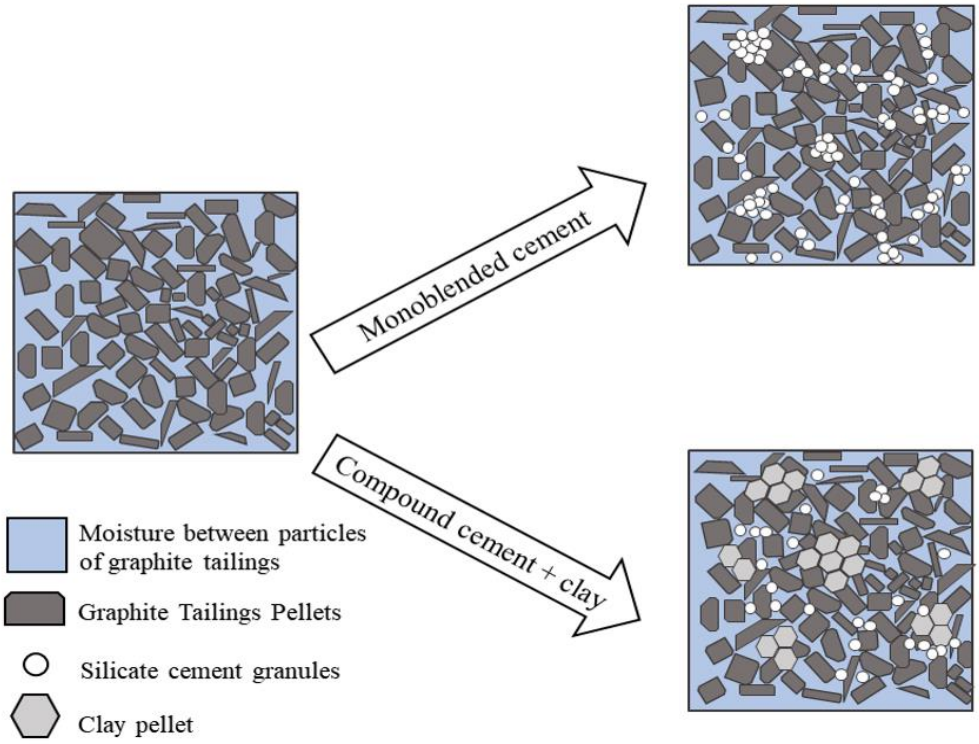

Figure 15. GT–Clay cluster schematic.

4. Conclusions

The following conclusions were obtained by exploring the laws affecting the macroscopic and microscopic changes in the cementitious materials by blending cement and clay in graphite tailings:

(1) For GT, the compressive strength increased gradually with the increase in the cement dosage and age. The maximum compressive strength reached 6.67 Mpa, and the minimum compressive strength reached 0.37 Mpa. For 90% GT–Clay, the compressive strength decreased with the increase in the clay substitution rate. Moreover, 95% GT–Clay maintained a compressive strength of around 0.5 Mpa with the increase in the clay substitution rate.

(2) As the clay replacement rate progressively increased, there was a critical value between the 90% GT-Clay permeability coefficient and the clay replacement rate, with a gradual increase in the permeability coefficient when the clay replacement rate was greater than 10 percent, but this still met the requirements of the first category of general industrial solid waste landfill standards (GB18599–2020) when the permeability was less than 10^{-5}. In addition, the permeability of 95% GT–Clay was directly proportional to the clay replacement rate and was greater than 10^{-5}; thus, it is recommended that 90% GT–50% Clay be chosen as the best replacement. In addition, lime, gypsum, and silica fume can improve the permeability of GT–Clay.

(3) According to the heavy metal analysis of the graphite tailing sand, heavy metal elements such as barium, arsenic, and nickel were more active, and nickel and copper showed a significant strong positive correlation at the 0.05 level, with the sources being highly homologous. Cement had a good curing effect on graphite tailing sand, which greatly reduced the leaching of heavy metals. The greater the amount of cement, the lower the leaching concentration of heavy metals in GT, which was lower than the highest standard for the leaching concentrations of national hazardous waste. For GT curing materials, the amounts of Cd, As, and Ni are much higher than the screening value of soil pollution risk in agricultural land, which is a potential source of contamination, and we should pay attention to its leaching and releasing pattern.

(4) The microstructure shows that there were obvious hydration products that generate C–S–H gel in 90% GT–Clay specimens after mixing with cement, which filled in the interstices of agglomerates, reduced the spacing between particles, and improved the denseness of the specimens. This was the main reason for the increase in compressive strength and impermeability and the decrease in the concentration of heavy metal leaching.

The results of this study can provide a reference for the mechanical mechanism study of GT–Clay for the preparation of graphite tailing sand curing compounds with high dosages. In the future, cement doping can be used as a basis for these curing compounds. In addition, the results obtained from mechanical and durability property testing can lay the foundation for the feasibility evaluation of GT–Clay preparation. The relationship between cement content, mechanical properties, and durability can be established, and the optimal solution can be applied to actual projects.

Author Contributions: Conceptualization, R.J. and Z.W.; methodology, R.J. and Z.W.; software, R.J. and Z.W.; validation, R.J. and Z.W.; formal analysis, R.J.; investigation, R.J. and Z.W.; resources, R.J. and Z.W.; data curation, R.J.; writing—original draft preparation, R.J.; writing—review and editing, Z.W.; visualization, R.J. and Z.W.; supervision, Z.W.; project administration, Z.W.; funding acquisition, Z.W. All authors have read and agreed to the published version of the manuscript.

Funding: This study was supported by a research project of the Heilongjiang Provincial Key Research and Development Program under the guidance category (GZ20220138, Z20210061) and a scientific research project of the Department of Ecology and Environment of Heilongjiang Province (HST2022GF004).

Data Availability Statement: Data are contained within the article.

Conflicts of Interest: The authors declare no conflicts of interest.

References

1. Chen, Y.; Li, S.; Lin, S. Promising energy-storage applications by flotation of graphite ores: A review. *Chem. Eng. J.* **2023**, *454*, 139994. [CrossRef]
2. Androulidakis, C.; Koukaras, E.N.; Hadjinicolaou, M. Non-Eulerian behavior of graphitic materials under compression. *Carbon* **2019**, *138*, 227–233. [CrossRef]
3. Case, G.N.D.; Karl, S.M.; Regan, S.P.; Johnson, C.A.; Ellison, E.T.; Caine, J.S.; Holm-Denoma, C.S.; Pianowski, L.S.; Marsh, J.H. Insights into the metamorphic history and origin of flake graphite mineralization at the Graphite Creek graphite deposit, Seward Peninsula, Alaska, USA. *Miner. Depos.* **2023**, *58*, 939–962. [CrossRef]
4. Chehreh Chelgani, S.; Rudolph, M.; Kratzsch, R.; Sandmann, D.; Gutzmer, J. A Review of Graphite Beneficiation Techniques. *Miner. Process. Extr. Metall. Rev.* **2016**, *37*, 58–68. [CrossRef]
5. Cui, N.; Sun, L.; Bagas, L. Geological characteristics and analysis of known and undiscovered graphite resources of China. *Ore Geol. Rev.* **2017**, *91*, 1119–1129. [CrossRef]
6. Luo, G.; Han, Z.; Xiong, J.; He, Y.; Liao, J.; Wu, P. Heavy metal pollution and ecological risk assessment of tailings in the Qinglong Dachang antimony mine, China. *Environ. Sci. Pollut. Res.* **2021**, *28*, 33491–33504. [CrossRef]
7. Jing, X.; Xiaomin, W.; Zhongrui, W.; Shuquan, X.; Hongbo, L. Investigations on influencing factors of resistivity measurement for graphite tailings concrete. *Cem. Concr. Compos.* **2021**, *123*, 104206.
8. Sharma, R.S.; Al-Busaidi, T.S. Groundwater pollution due to a tailings dam. *Eng. Geol.* **2001**, *60*, 235–244. [CrossRef]
9. Yujie, H.; Qian, Z.; Wenjie, W.; Jie, H.; Haisheng, L. The multi-media environmental behavior of heavy metals around tailings under the influence of precipitation. *Ecotoxicol. Environ. Saf.* **2023**, *266*, 115541.
10. Liu, H.; Xue, J.; Li, B.; Wang, J.; Lv, X.; Zhang, J. Effect of graphite tailings as substitute sand on mechanical properties of concrete. *Eur. J. Environ. Civ. Eng.* **2020**, *26*, 2635–2653. [CrossRef]
11. Yang, X.; Fan, Z.; Xu, J.; Lin, J.; He, Y.; Wang, D.; Liu, P. Investigation of graphite tailings as a substitute for filler in asphalt mastics. *Int. J. Pavement Eng.* **2023**, *24*, 2172578. [CrossRef]
12. Yulong, F.; Yuqing, J.; Jing, M.; Junhao, L.; Zhi, W.; Bin, W.; Xuzhong, G. Lithium-ion transfer strengthened by graphite tailings and coking coal for high-rate performance anode. *Chem. Eng. J.* **2022**, *442*, 136184.
13. Hu, S.; Li, D.; Li, Y.; Guo, Q.; Tian, D.; Zhang, L.; Li, H. Preparation of Foamed Ceramics from Graphite Tailings Using A Self-Foaming Method. *Minerals* **2023**, *13*, 521. [CrossRef]
14. Hourui, D.; Hongbo, L.; Bochen, L.; Zhongrui, W.; Hongshuai, G. Mechanical Properties and Mechanism Analysis of Graphite Tailings Environment-Friendly Concrete. *Materials* **2022**, *15*, 8870.
15. Jiantao, L.; Ming, Z.; Wenxin, J. Characteristics of the cement-solidified municipal solid waste incineration fly ash. *Environ. Sci. Pollut. Res. Int.* **2018**, *25*, 36736–36744.

16. Tong, Z.; Siqi, Z.; Huifen, Y.; Wen, N.; Jia, L.; Ge, Z.; Guoxiang, T. Influence on fine lead–zinc tailings solidified/stabilised by clinker-free slag-based binder. *J. Environ. Chem. Eng.* **2022**, *10*, 108692.
17. Wu, F.; Liu, X.; Qu, G.; Ning, P.; Jin, C.; Cui, Q.; Ren, Y.; He, M.; Yang, Y.; Li, J. Solidification and stabilization of harmful elements in antimony tailings and synergistic utilization of multiple solid wastes. *Cem. Concr. Compos.* **2022**, *133*, 104718. [CrossRef]
18. Sun, Y.; Zhao, Y.; Wan, X.; Qiu, J.; Wu, P.; Sun, X. Stabilization/solidification of lead- and cadmium-containing tailings for cemented paste backfill by using clinker-free binders. *Constr. Build. Mater.* **2022**, *359*, 129469. [CrossRef]
19. Althoey, F.; Elaal, A.K.A.; Shoukry, H.; Hakeem, I. Performance of Cement Mortars Containing Clay Exposed to High Temperature. *Arab. J. Sci. Eng.* **2022**, *47*, 591–599. [CrossRef]
20. Andrade, F.A.; Al-Qureshi, H.A.; Hotza, D. Measuring the plasticity of clays: A review. *Appl. Clay Sci.* **2011**, *51*, 1–7. [CrossRef]
21. Wang, S.; Gainey, L.; Mackinnon, I.D.; Allen, C.; Gu, Y.; Xi, Y. Thermal behaviors of clay minerals as key components and additives for fired brick properties: A review. *J. Build. Eng.* **2023**, *66*, 105802. [CrossRef]
22. Dang, J.; Du, H.; Dai Pang, S. Hydration, strength and microstructure evaluation of eco-friendly mortar containing waste marine clay. *J. Clean. Product.* **2020**, *272*, 122784. [CrossRef]
23. Argane, R.; Benzaazoua, M.; Hakkou, R.; Bouamrane, A. Reuse of base-metal tailings as aggregates for rendering mortars: Assessment of immobilization performances and environmental behavior. *Constr. Build. Mater.* **2015**, *96*, 296–306. [CrossRef]
24. *JGJ/T 70-2009*; Standard Test Methods for Basic Properties of Building Mortar. China Architecture & Building Press: Beijing, China, 2009.
25. *GB/T 50123-2019*; Geotechnical Test Method Standards. Standards Press of China: Beijing, China, 2019.
26. *GB 5085.3-2007*; Hazardous Waste Identification Criteria Leaching Toxicity Identification. AQSIQ: Beijing, China, 2007.
27. *HJ/T 299-2007*; Solid Waste Leaching Toxicity Leaching Methods. Sulfuric Acid-Nitric Acid Method. Institute of Solid Waste Pollution Control Technology, China Academy of Environmental Sciences (CAES): Beijing, China, 2007.
28. Nazile, U. The significance of scanning electron microscopy (SEM) analysis on the microstructure of improved clay: An overview. *Open Geosci.* **2021**, *13*, 197–218.
29. Ahmed, H.U.; Mohammed, A.S.; Faraj, R.H.; Abdalla, A.A.; Qaidi, S.M.; Sor, N.H.; Mohammed, A.A. Innovative modeling techniques including MEP, ANN and FQ to forecast the compressive strength of geopolymer concrete modified with nanoparticles. *Neural Comput. Appl.* **2023**, *35*, 12453–12479. [CrossRef]
30. Quan, P.; Sun, Q.; Xu, Z.; Shi, M.; Gao, Z.; Wang, D.; Liu, D.; Yang, L.; Song, S. Study on the mechanical properties and strength formation mechanism of high-volume graphite tailings concrete. *J. Build. Eng.* **2024**, *84*, 108500. [CrossRef]
31. Mention, S.A.; Arsalan, R.; Khan, S.; Lo, T.Y. Utilization of Pakistani bentonite as partial replacement of cement in concrete. *Constr. Build. Mater.* **2012**, *30*, 237–242.
32. *GB 18599-2020*; General Industrial Solid Waste Storage and Landfill Pollution Control Standards. PRC State General Organization for the Protection of the Environment (GOPE): Beijing, China, 2020.
33. Ke, Y.; Shen, Y.; Qing, C.; Hu, K.; Wang, S.; Chen, Q.; Guan, H. Mechanical properties and microstructure evolution of cemented tailings backfill under seepage pressure. *Front. Mater.* **2022**, *8*, 818698. [CrossRef]
34. Angulo, S.C.; Guilge, M.S.; Quarcioni, V.A.; Cincotto, M.A.; Nobre, T.R.S.; Poellmann, H. The role of calcium silicates and quicklime on the reactivity of rehydrated cements. *Constr. Build. Mater.* **2022**, *340*, 127625. [CrossRef]
35. Yishun, L.; Sichun, W.; Kejin, W.; Al, Q.S.; Shihui, W.; Zhengxia, Y.; Pengfei, X.; Shengwen, T. A study on the hydration of calcium aluminate cement pastes containing silica fume using non-contact electrical resistivity measurement. *J. Mater. Res. Technol.* **2023**, *24*, 8135–8149.
36. Zezulová, A.; Rybová, A.; Staněk, T. Hydration of clinkers doped with baryte with and without addition of gypsum. *J. Therm. Anal. Calorim.* **2019**, *138*, 1945–1952. [CrossRef]
37. Liao, Y.; Yao, J.; Deng, F.; Li, H.; Wang, K.; Tang, S. Hydration behavior and strength development of supersulfated cement prepared by calcined phosphogypsum and slaked lime. *J. Build. Eng.* **2023**, *80*, 108075. [CrossRef]
38. He, X.; Jun, W.; Qitai, J. Mechanical properties and drying shrinkage of graphite tailing-basalt fiber cement mortar. *Constr. Build. Mater.* **2023**, *409*, 133898.
39. Ye, L. Effect of post-fire curing and silica fume on permeability of ultra-high performance concrete. *Constr. Build. Mater.* **2021**, *290*, 123175.
40. Jiang, Z.; Yang, S.; Luo, S. Source analysis and health risk assessment of heavy metals in agricultural land of multi-mineral mining and smelting area in the Karst region—A case study of Jichangpo Town, Southwest China. *Heliyon* **2023**, *9*, e17246. [CrossRef] [PubMed]
41. Zhao, S.; Xia, M.; Yu, L.; Huang, X.; Li, D. Optimization for the preparation of composite geopolymer using response surface methodology and its application in lead-zinc tailings solidification. *Constr. Build. Mater.* **2021**, *266*, 120969. [CrossRef]
42. *GB 15618-2018*; Soil Environmental Quality Risk Control Standard for Soil Contamination of Agricultural Land. China Environmental Science Publishing House: Beijing, China, 2018.
43. Baek, J.W.; Choi, A.E.S.; Park, H.S. Solidification/stabilization of ASR fly ash using Thiomer material: Optimization of compressive strength and heavy metals leaching. *Waste Manag.* **2017**, *70*, 139–148. [CrossRef]
44. Liu, H.; Liu, K.; Lan, Z.; Zhang, D. Mechanical and Electrical Characteristics of Graphite Tailing Concrete. *Adv. Mater. Sci. Eng.* **2018**, *2018*, 9297628. [CrossRef]

45. Chen, Z.; Ben, L.; Fanghong, W.; Ying, Y.; Yu, Z.; Hu, X. Research on modification of mechanical properties of recycled aggregate concrete by replacing sand with graphite tailings. *Rev. Adv. Mater. Sci.* **2022**, *61*, 493–512.
46. Zhang, Y.; Pan, F.; Wu, R. Study on the performance of FGD gypsum-metakaolin-cement composite cementitious system. *Constr. Build. Mater.* **2016**, *128*, 1–11. [CrossRef]